AIMS Mathematics

AIMS Mathematics, 11(6): 18970–18993.
DOI: 10.3934/math.2026772
Received: 13 March 2026
Revised: 02 June 2026
Accepted: 16 June 2026
Published: 26 June 2026

https://www.aimspress.com/journal/Math

Research article

Two finite difference schemes to enhance nanofluid stability and heat transfer: Bioconvection with motile microorganisms in non-Darcy media

Sahin Ahmed[1], Nava Jyoti Hazarika[2], Joaquin Zueco[3,*] and Joaquín Solano Ramírez[4]

[1] Department of Mathematics, Rajiv Gandhi Central University, Rono Hills, Itanagar, Arunachal Pradesh-791112, India
[2] Department of Mathematics, Tyagbir Hem Baruah College, Jamugurihat, Sonitpur-784189, Assam, India
[3] Department of Thermal Engineering and Fluids, Universidad Politécnica de Cartagena, Campus Muralla del Mar, 30202 Cartagena, Spain
[4] Department of Mechanical Engineering, Materials and Manufacturing, Universidad Politécnica de Cartagena, Campus Muralla del Mar, 30202 Cartagena, Spain

* **Correspondence:** Email: joaquin.zueco@upct.es; Tel: 0033-968 325989.

Abstract: This study investigates steady magnetohydrodynamic bioconvective flow of a Prandtl-type nanofluid containing motile microorganisms over an inclined stretching sheet embedded in a non-Darcy porous medium. The governing nonlinear similarity equations incorporate magnetic effects, Brownian diffusion, thermophoresis, and Forchheimer drag, thus representing the coupled interaction between momentum, heat, nanoparticle concentration, and microorganism transport. The resulting boundary-value problem is solved using two independent numerical approaches: a collocation-based solver (bvp4c) and the Network Simulation Method (NSM), formulated through an electrical analogy framework. Grid refinement and cross-validation confirm numerical consistency between both methods. The results indicate that magnetic and porous resistance parameters suppress momentum transport while modifying thermal and microorganism distributions within the boundary layer. Variations in bioconvection and inclination parameters significantly influence surface shear stress, heat transfer, and mass diffusion characteristics. The study demonstrates that NSM provides a stable and conservative computational framework for strongly nonlinear multiphysics boundary-layer systems, thus supporting its applicability to complex bioconvective nanofluid configurations.

Keywords: motile microorganism; prandtl nanofluid; non-Darcy medium; Brownian motion; bioconvection; stretching sheet; network model
Mathematics Subject Classification: 35G30, 35Q30, 65N06, 65N12, 65N22, 65N50

1. Introduction

Bioconvection arises from the collective motion of motile microorganisms suspended in a fluid, leading to the formation of macroscopic convective patterns driven by density gradients. Biswas et al. [1] examined recent advances in understanding bioconvective dynamics, which is a hydrodynamic instability phenomenon that arises from the collective motion of motile microorganisms within porous media. Its relevance spans applications such as wastewater treatment, bioreactor optimization, microfluidic transport systems, and enhanced mixing strategies in porous structures.

In recent years, the incorporation of nanoparticles into base fluids has led to the development of nanofluids with enhanced thermal transport characteristics. However, despite improved thermal conductivity, nanoparticle aggregation and sedimentation remain significant challenges that affect long-term stability. The introduction of motile microorganisms into nanofluids has been proposed as a potential mechanism to promote microscale mixing, thereby improving both the suspension stability and the mass transport efficiency. Consequently, this interplay between nanofluid transport and bioconvective mechanisms has attracted considerable research attention.

Several studies have investigated bioconvective nanofluid flow in porous media under various rheological and physical assumptions. Bég et al. [2] examined mixed convection bioconvection in porous media saturated with nanofluids containing oxytactic microorganisms, thus emphasising the role of microbial motion in heat transfer enhancement. Priyadharsini and Gururaj [3] studied the non-Newtonian behavior of blood in the presence of drug nanoparticles and microbes with magnetic and thermal radiation effects. Waqas et al. [4] explored Darcy–Forchheimer bioconvective nanofluid flow over stretching geometries with slip effects, including thermal radiation. Ahmad et al. [5] analyzed bioconvection induced by gyrotactic microorganisms in porous media, while Wang et al. [6] studied Prandtl nanofluid Darcy–Forchheimer flow over inclined sheets. Yaseen et al. [7] incorporated the Cattaneo–Christov heat flux model to analyze Darcy–Forchheimer radiative nanofluid flow over a stretching surface.

In recent years, the incorporation of nanoparticles into base fluids has led to the development of nanofluids with enhanced thermal transport characteristics. However, despite their enhanced thermal conductivity, nanoparticle aggregation and sedimentation remain significant challenges that affect long-term stability. The introduction of motile microorganisms into nanofluids has been proposed as a mechanism to promote microscale mixing, thereby improving both the suspension stability and the mass transport efficiency. Consequently, this coupling between nanofluid dynamics and bioconvective mechanisms has attracted considerable research attention.

The influence of magnetic fields and non-Newtonian rheology on bioconvective transport has also been widely reported. Khan et al. [8] investigated magnetohydrodynamic (MHD) boundary-layer flow of nanofluids containing gyrotactic microorganisms, whereas Khan et al. [9] examined magnetohydrodynamic Prandtl fluid flow in the presence of stratification and heat generation. Das and Ahmed [10] employed a finite difference approach to model bioconvective Prandtl nanofluid flow over an inclined stretching sheet, while Hazarika and Ahmed [11] extended the analysis to non-Darcy porous media. Additional contributions addressing chemically reactive, radiative, and thermally stratified Prandtl nanofluid flows have been reported by Rasheed et al. [12], Abbas et al. [13], Bilal and Nazeer [14], and Bhattacharyya [15].

More complex rheological models, including Casson and micropolar fluids, have been incorporated into bioconvective frameworks by Ghosh et al. [16], Jawad et al. [17], and Siddiqui et al. [18], thereby building on the micropolar fluid framework. Studies on viscoelastic and Maxwell-type nanofluids containing microorganisms have been reported by Habib et al. [19] and Batool et al. [20], while non-similar and chemically reactive configurations were analyzed by Farooq et al. [21–23]. Magnetized bioconvective micropolar nanofluids in porous enclosures were investigated by Mansour et al. [24], and scaling group analyses in porous media were presented by Naganthran et al. [25]. Recent work by Das et al. [26] considered nano-encapsulated phase change material (NEPCM)–water nanofluid bioconvection over inclined cylinders using extended Darcy models. Khader and Adel [27] used the advanced modified decomposition method (MDM) to study the Reiner–Philippoff nanofluid flow over a stretching sheet considering diffusion and first order velocity slip. Nima and Hannan [28] investigated the mixed convection flow over a vertical thin needle with variable surface heat, mass, and microbial flux, thereby incorporating the influence of gyrotactic microorganisms.

The recent importance of Williamson nanofluids has grown significantly in advanced research on heat transfer, energy, and bioengineering due to their non-Newtonian behavior, high thermal efficiency, and flow control through magnetic fields and nanoparticles. They exhibit a higher thermal conductivity than conventional fluids, thus allowing heat to dissipate more rapidly in compact systems. Jawad et al. [29] studied the dynamics of activation energy and gyrotactic microorganisms in a Williamson radiative nanofluid with Soret and Dufour bounded by a nonlinearly stretching porous surface. Sankari et al. [30] obtained an analytical solution of MHD bioconvection Williamson nanofluid flow over an exponentially stretching sheet by analyzing the effect of viscous dissipation and gyrotactic microorganism. Finally, Khader et al. [31] examined the 2D, steady-state flow of a non-Newtonian nanofluid past an impermeable stretching sheet, thereby incorporating temperature-dependent density, nonlinear rheology, nanoparticle transport mechanisms (thermophoresis/Brownian motion), and thermal radiation using merged Fibonacci-Lucas polynomials combined with least squares approximation, transforming the equations into algebraic form solved via the Newton iteration method.

Although the physical modeling of bioconvective nanofluid systems has been extensively explored, most investigations rely on conventional numerical techniques, typically shooting methods or collocation-based solvers such as MATLAB's bvp4c. Numerical reliability is typically solely assessed through grid refinement checks, and limited attention has been devoted to alternative computational frameworks suited to strongly nonlinear multiphysics problems. The Network Simulation Method (NSM), originally developed from thermoelectric analogies and implemented using circuit simulation software such as SPICE [32,33], offers a fundamentally distinct numerical strategy. By mapping the governing differential equations onto equivalent electrical networks, the NSM exploits Kirchhoff's current laws to enforce conservation principles while accommodating nonlinear source terms through controlled current sources representing the nonlinear coupling terms. In this respect, the NSM operates as a spatially discretized scheme analogous to finite differences but derived entirely from circuit conservation laws.

Motivated by this methodological gap, the present study investigates the steady two-dimensional magnetohydrodynamic flow of a Prandtl-type nanofluid containing motile microorganisms over an inclined stretching sheet embedded in a non-Darcy porous medium with Forchheimer drag effects. The governing equations incorporate Brownian diffusion, thermophoretic transport, Lorentz force effects, and microorganism density dynamics. By applying similarity transformations, the system is reduced to a strongly coupled nonlinear set of ordinary differential equations. The resulting boundary-value problem is solved using two independent computational approaches: (i) a collocation-based bvp4c solver and (ii) an NSM formulation implemented within an electrical-circuit framework.

The analysis investigates the influence of the magnetic parameter, bioconvection Lewis number, Forchheimer number, inclination angle, and Prandtl fluid parameter on the velocity, temperature, nanoparticle concentration, and microorganism density distributions. Engineering quantities, including the skin-friction coefficient, Nusselt number, and Sherwood number, are evaluated to quantify transport performance. Particular emphasis is placed on cross-validating the NSM approach against the conventional solver and assessing its numerical robustness in the presence of strong nonlinear coupling.

In view of the extensive literature on bioconvective nanofluid transport [1–31], the novelty of the present work does not solely lie in the inclusion of additional physical parameters within an established modeling framework. Rather, its principal contribution is methodological in nature.

Specifically, this study accomplishes the following:

1. Develops a consistent electrical-network representation of the nonlinear similarity equations governing Prandtl-type bioconvective nanofluid flow in a non-Darcy porous medium.
2. Demonstrates the practical implementation of the NSM using circuit-simulation tools originally developed for nonlinear electronic systems.
3. Provides a direct computational cross-validation between the NSM and a standard collocation-based boundary-value solver.
4. Extends previous NSM heat-transfer applications to a coupled bioconvective nanofluid configuration involving magnetic, porous-medium, and non-Newtonian effects.

The developed network model and the physical problem are governed by the same finite difference equations in space, thereby encompassing both the volume of the elementary cell and the boundary conditions, so the equivalence between them is direct. However, in non-stationary problems, time remains a continuous variable in the design model. This means that spatial discretization is explicit and controllable, while time integration is handled automatically and continuously by the circuit solver. This method solves non-linear, coupled, or uncoupled differential equations without any assumptions regarding linearization of the variables, a significant edge over classical finite difference or finite element approaches that often require linearization of non-linear terms. Accordingly, the core contribution of this work is the demonstration that the NSM constitutes a viable and robust computational alternative for strongly nonlinear multiphysics boundary-layer problems involving bioconvective nanofluids in porous media.

The study of bioconvection with motile microorganisms in non-Darcy porous media has significant practical relevance in biomedical engineering, biofuel production, environmental remediation, and microbial transport processes. Understanding how microorganism-induced convection interacts with complex porous structures can improve the design of bioreactors, filtration systems, and enhanced oil recovery techniques. Moreover, the inclusion of non-Darcy effects provides a more realistic description of high-velocity transport in porous materials encountered in industrial and natural systems.

2. Mathematical formulation

Figure 1 illustrates the physical configuration of the present model, which describes the bioconvective boundary-layer flow of a Prandtl nanofluid over an inclined stretching surface embedded in a porous medium. The sheet is inclined at an angle γ to the vertical and linearly stretches along the x-direction with velocity $u_w = ax$, where $a > 0$ is the stretching rate constant. A uniform magnetic field of strength B_0 is normally applied to the surface.

The coordinate system is chosen such that the x-axis lies along the stretching sheet, while the y-axis is taken perpendicular to it. Due to stretching, a momentum boundary layer develops near the surface, followed successively by the thermal boundary layer, concentration boundary layer, and microorganism density boundary layer, which represent the transport of velocity, temperature, nanoparticle concentration, and motile microorganisms, respectively.

The surrounding medium is porous, allowing fluid to pass through interconnected pores, which influences the resistance to motion. Nanoparticles are uniformly suspended in the base fluid, while gyrotactic microorganisms are included to stabilize the suspension and generate bioconvection. The interaction of magnetic force, buoyancy, porous resistance, and microorganism motion significantly affects the transport characteristics of the flow.

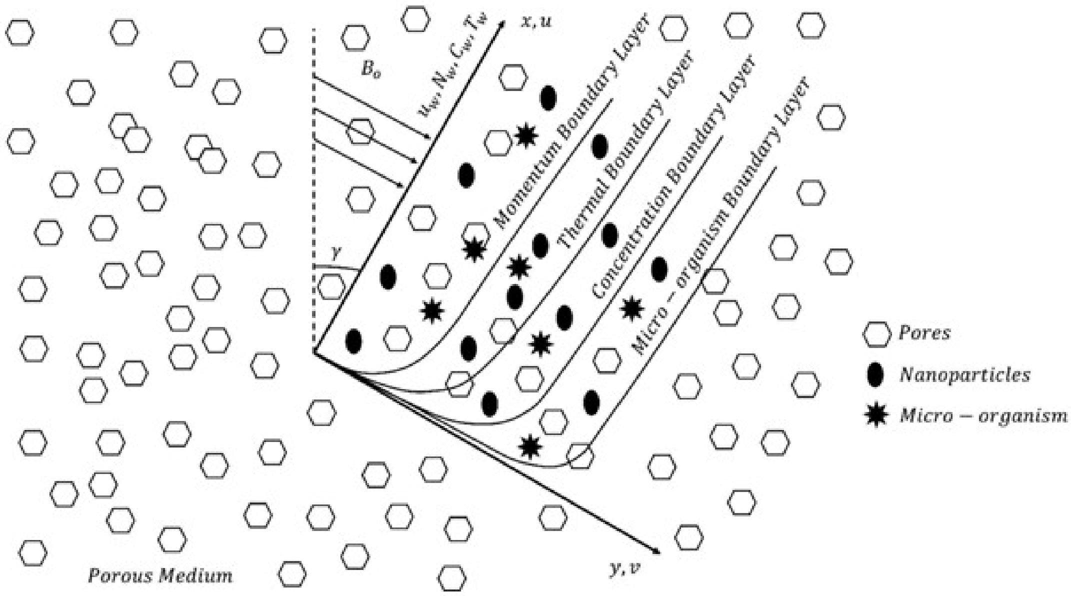

Figure 1. Geometry of bio-convection model.

Equation (1) represents the non-Newtonian shear stress tensor (τ^*, this defines how the fluid resists deformation when subjected to force) for a Prandtl fluid model adapted for multi-dimensional boundary layer flow:

$$\tau^* = \frac{A\,si\quad^{-1}\left\{\frac{1}{C}\left[\left(\frac{\partial u}{\partial y}\right)^2 + \left(\frac{\partial v}{\partial y}\right)^2\right]^{0.5}\right\}}{\left[\left(\frac{\partial u}{\partial y}\right)^2 + \left(\frac{\partial v}{\partial y}\right)^2\right]}, \tag{1}$$

where A and C are Prandtl fluid parameters; these are characteristic material constants of the Prandtl fluid model, where A is related to the fluid's consistency or flow behavior index and C is a reference shear rate parameter.

The fundamental equations which govern the fluid flow dynamics are formulated as follows:

$$\frac{\partial u}{\partial x}+\frac{\partial v}{\partial y}=0, \tag{2}$$

$$u\frac{\partial u}{\partial x}+v\frac{\partial u}{\partial y}=\frac{A\,\nu}{C}\left(\frac{\partial^2 u}{\partial y^2}\right)+\frac{A\,\nu}{2C^3}\left(\frac{\partial u}{\partial y}\right)^2\left(\frac{\partial^2 u}{\partial y^2}\right)-\frac{\sigma\,B_o^2(x)}{\rho}sin^2(\gamma)u-\frac{\nu}{K}\,u-Fu^2+$$
$$g\,\beta_1\,\rho_f(1-C_\infty)(T-T_\infty)cos(\alpha)-g\left(\rho_p-\rho_f\right)(C-C_\infty)cos(\alpha)-g\gamma^*\left(\rho_m-\rho_f\right)(N-N_\infty)cos(\alpha), \tag{3}$$

$$u\frac{\partial T}{\partial x}+v\frac{\partial T}{\partial y}=\frac{k_t}{\rho C_p}\frac{\partial^2 T}{\partial y^2}+\tau\left[D_B\frac{\partial C}{\partial y}\frac{\partial T}{\partial y}+\frac{D_T}{T_\infty}\left(\frac{\partial T}{\partial y}\right)^2\right]+\frac{\sigma}{\rho C_p}B_o^2(x)\,sin^2(\gamma)\,u^2, \tag{4}$$

$$u\frac{\partial C}{\partial x}+v\frac{\partial C}{\partial y}-D_B\frac{\partial^2 C}{\partial y^2}=\frac{D_T}{T_\infty}\frac{\partial^2 T}{\partial y^2}, \tag{5}$$

$$u\frac{\partial N}{\partial x}+v\frac{\partial N}{\partial y}=\frac{d\,w_c}{C_f-C_0}\frac{\partial}{\partial y}\left(N\frac{\partial C}{\partial y}\right)+D_N\left(\frac{\partial^2 N}{\partial y^2}\right), \tag{6}$$

where u is the fluid velocity component in the x-direction (along the surface), v is the fluid velocity component in the y-direction (normal to the surface), ν is the kinematic viscosity of the base fluid, σ is the electrical conductivity of the fluid, B_o is the constant magnetic field strength, γ is the inclination angle of the magnetic field, ρ is the density of the fluid, ρ_p is the density of the nanoparticles, C is the local concentration of nanoparticles, γ^* is the average volume of a microorganism, K is the permeability of the porous medium, F is the Non-Darcy empirical inertia coefficient, g is the acceleration due to gravity, β_1 is the volumetric thermal expansion coefficient, T is the local temperature of the fluid, T_∞ is the free-stream temperature, C_∞ is the ambient nanoparticle concentration, α is the inclination angle of the boundary surface, ρ_m is the density of a microorganism, N is the local concentration of motile microorganisms, N_∞ is the free-stream concentration of microorganisms, k_t is thermal conductivity of the fluid, C_p is the specific heat capacity at constant pressure, τ represents the capacity of heat relation of the fluid and nanoparticles ($\tau=(\rho C)_p/(\rho C)_f$), D_B is the Brownian diffusion coefficient, D_T is the thermophoretic diffusion coefficient, d is the chemotaxis constant (also known as the cell swimming speed coefficient), w_c is the maximum cell swimming speed, C_f is the reference or free-stream nanoparticle concentration, C_o is the nanoparticle concentration at the surface boundary, and D_N is the diffusivity coefficient of the motile microorganisms.

The boundary conditions are as follows:

At the wall, $y = 0$:

All conditions linearly vary with x, which is the standard form required by similarity solutions for stretching flows:

- $u=\in u_w=a\,x$: the wall moves with a velocity proportional to the distance x from the leading edge (linear stretching); $\in$ is a slip parameter that allows for the modeling of partial-slip walls. (7a)

- $v = v_0$: non-zero normal velocity at the wall, modeling suction ($v_0 < 0$) or fluid injection ($v_0 > 0$), a standard tool for boundary layer control. v_0 is the constant mass flux velocity at the wall surface. (7b)
- $T_f = T_0 + a_1 x$: wall temperature linearly varying with x, capturing non-uniform heating of the plate. (7c)
- $C = C_f = C_0 + a_2 x$: nanoparticle concentration at the wall, also non-uniform. Models the surface as a source or sink of nanoparticles. (7d)
- $N = N_f = N_0 + a_3 x$: microorganism density prescribed at the wall. (7e)

The parameters a_1, a_2, and a_3 are linear proportionality coefficients.
At infinity, $y \to \infty$.
These conditions reflect that the fluid reaches the undisturbed free-stream state far from the plate:

- $u \to 0$: the longitudinal velocity decays to zero outside the boundary layer (quiescent free stream, or already absorbed into u_w). (7f)
- $T = T_0 + d_1 x,\ C = C_0 + d_2 x,\ N = N_0 + d_3 x$: free-stream temperature, concentration, and microorganism density, also with linear variation in x to remain consistent with the similarity solution. The coefficients d_1, d_2, and d_3 are constants. (7g)

To renovate the leading system of equations into a more manageable form, the following similarity transformations are applied (Eq (8)). This allows transforming a system of partial differential equations (dependent on x and y) into a system of ODEs only dependent on η, which greatly simplifies the numerical resolution:

$$\left\{\begin{array}{l} \psi = \sqrt{a v x} f(\eta), \eta = \left(\frac{a}{v}\right)^{\frac{1}{2}} y, u = \frac{\partial \psi}{\partial y} = a x f'(\eta), \\ v = -\frac{\partial \psi}{\partial x} = -\sqrt{a v x} f(\eta), \theta(\eta) = \frac{T - T_\infty}{T_f - T_0}, \\ \phi(\eta) = \frac{C - C_\infty}{C_f - C_0}, \chi(\eta) = \frac{N - N_\infty}{N_f - N_0}, \end{array}\right\}; \tag{8}$$

where ψ is the stream function, and η is the similarity variable.
Based on Eq (8), the leading equations are transmuted into the following reduced ordinary differential equations (ODEs):

$$\left\{\begin{array}{l} f'''\delta\left(1 + \beta_1 f''^2\right) + f f'' - M\, Sin^2 \gamma\, f' - \\ K_p f' + (Fr + 1) f'^2 + w(\theta - Nr\phi - Rb\chi)\cos(\alpha) \end{array}\right\} = 0, \tag{9}$$

$$\frac{1}{Pr}\theta'' - f'\theta + +f\theta' + Nb\,\theta\,\phi + Nt\,\theta'^2 + MEc\,f'^2 = 0, \tag{10}$$

$$\phi'' - Sc\left(f'\phi + f\phi'\right) + \frac{Nt}{Nb}\theta'' = 0, \tag{11}$$

$$\chi'' - Lb\chi f' + Lb\chi' f - Pe\left(\phi'\chi' + \chi\phi'' + \Omega\phi''\right) = 0. \tag{12}$$

The transmuted constraints are as follows:

$$\begin{bmatrix} \eta = 0: \begin{Bmatrix} f(\eta) = S, f'(\eta) = \in, \theta(\eta) = 1 - S_1, \\ \phi(\eta) = 1 - S_2, \chi(\eta) = 1 - S_3 \end{Bmatrix} \\ \eta \to \infty: \{f'(\eta) \to 0, \theta(\eta) \to 0, \chi(\eta) \to 0\} \end{bmatrix}, \tag{13}$$

where

$$\begin{Bmatrix} \delta = \frac{A}{\tilde{C}}, \beta = \frac{a^3x^2}{2\tilde{C}^2\nu}, M = \frac{\sigma B^2(x)}{\rho a}, K_p = \frac{\nu}{Ka}, Fr = \frac{C_b x}{\sqrt{K}}, Ec = \frac{U_w^2}{C_p(T_f - T_0)} \\ w = \frac{g\beta_1\rho_f}{U_w^2}(T_f - T_0)(1 - C_\infty), Nr = \frac{(\rho_p - \rho_f)(C_f - C_0)}{\beta_1\rho_f(T_f - T_0)(1 - C_\infty)}, Pr = \frac{\rho C_p \nu}{k_t}, \\ Rb = \frac{(\rho_m - \rho_f)(N_f - N_0)}{\beta_1\rho_f(T_f - T_0)(1 - C_\infty)}, Nb = \frac{\tau D_B(C_f - C_0)}{\nu}, Nt = \frac{\tau D_T(T_f - T_0)}{T_\infty \nu}, \\ Lb = \frac{\nu}{D_B}, Pe = \frac{dw_c}{D_N}, \Omega^* = \frac{N_\infty}{N_f - N_0}, S_1 = \frac{d_1}{a_1}, S_2 = \frac{d_2}{a_2}, S_3 = \frac{d_3}{a_3}, \end{Bmatrix}, \tag{14}$$

where δ is the Prandtl fluid parameter (where A and $\tilde{C}$ are constants), β is the Prandtl-Eyring fluid parameter, M is the magnetic Parameter, K_p is the porous permeability parameter, C_b is the drag coefficient, Fr is the Forchheimer number, Ec is the Eckert number, w is the mixed convection parameter, Nr is the nanofluid buoyancy ratio parameter, Pr is the Prandtl number, Rb is the bioconvection buoyancy parameter, Nb is the Brownian motion parameter, Nt is the thermophoresis parameter, Lb is the bioconvection Lewis number, Pe is the bioconvection Péclet number, Ω^* is the microorganism concentration difference parameter, and S_1, S_2, S_3 are scalar stratification parameters (represent the thermal stratification, nanoparticle concentration stratification, and microorganism stratification parameters, respectively).

2.1. Engineering quantities

The velocity, thermal, molar, and bio-convection density gradients for the engineering variables that are related to physical characteristics may established as follows:

$$\begin{Bmatrix} C_{fx} = \frac{\tau_w}{\frac{1}{2}\rho_f U_w^2(x)}, Nu_x = \frac{xq_w}{k_t(T_w - T_\infty)}, \\ Sh_x = \frac{xq_m}{D_B(C - C_\infty)}, Nn_x = \frac{xq_n}{D_N(N - N_\infty)} \end{Bmatrix}, \tag{15}$$

$$\begin{Bmatrix} \tau_w = -\left(\frac{A}{\tilde{C}}\frac{\partial u}{\partial x} + \frac{A}{6\tilde{C}^3}\left(\frac{\partial u}{\partial y}\right)^3\right)_{y=0}, q_w = -k_t\left(\frac{\partial T}{\partial y}\right)_{y=0} \\ q_m = -D_B\left(\frac{\partial C}{\partial y}\right)_{y=0}, q_n = -D_N\left(\frac{\partial N}{\partial y}\right)_{y=0} \end{Bmatrix}. \tag{16}$$

Here, τ_w, q_w, q_m, and q_n represent the shear stress, heat flux, mass flux, and the flux of motile microorganism density, respectively. C_{fx} is the local skin friction coefficient, Nu_x is the local Nusselt number, Sh_x is the local Sherwood number, and Nn_x is the local density number of motile microorganisms.

By applying Eqs (8) and (16), Eq (15) is transformed into its dimensionless form as follows:

$$Re_x^{\frac{1}{2}} C_{fx} = -\left(\frac{\delta\beta}{3} f''^3(0) + \delta f''(0)\right), \tag{17}$$

$$Re_x^{-\frac{1}{2}} N u_x = -\left(\theta'(0)\right), \tag{18}$$

$$Re_x^{-\frac{1}{2}} S h_x = -\left(\phi'(0)\right), \tag{19}$$

$$Re_x^{-\frac{1}{2}} N n_x = -\left(\chi'(0)\right), \tag{20}$$

where $Re_x^{\frac{1}{2}} = \sqrt{\frac{U_w x}{\nu}}$ is the local Reynolds number.

2.2. Network simulation method of solution

The NSM is a numerical framework founded on the thermoelectric analogy between transport phenomena and the electrical circuit theory. Following the circuit-simulation philosophy introduced in SPICE-based solvers [32,33], the governing differential equations are transformed into an equivalent electrical-network representation. The methodology has been successfully applied to nonlinear heat-transfer and multiphysics problems [34–36] and has more recently been extended to bioconvective nanofluid systems in porous media by Das et al. [37]. In the present work, NSM is employed to solve the system of partial differential equations (9)–(12), subject to the boundary conditions given in (13), using classical numerical integration based on a finite-difference discretization scheme.

In NSM, multiple interconnected electrical networks are combined to represent the entire physical domain, while the boundary conditions are implemented through specialized electrical devices, such as current- or voltage-controlled sources. NSM is fundamentally based on the classical thermoelectric analogy between thermal and electrical variables. However, its ability to incorporate arbitrary nonlinearities into the model, by exploiting the well-established capabilities of electronic circuit simulators, distinguishes NSM from the conventional analogies commonly presented in standard textbooks. Within this analogy, the electrical current (*J*) corresponds to velocity, heat, and mass fluxes, whereas the electrical potential (*V*) is associated with velocity, temperature, and concentration fields.

We define the variable $\Omega = \frac{\partial f}{\partial \eta} = f'$ to reduce the third order partial differential momentum Eq (9) to a second order differential equation. Then, Eq (9) reduces to the following:

$$\begin{Bmatrix} \Omega''\delta(1+\beta_1\Omega'^2) + f\Omega' - M\sin^2\gamma\,\Omega \quad - \\ K_p\Omega + (Fr+1)\Omega^2 + w(\theta - Nr\phi - Rb\chi)\cos(\alpha) \end{Bmatrix} = 0. \tag{21}$$

Then, the discretized forms of Eqs (9) to (12) become the following:

$$\left\{\frac{\Omega_{i+1} + \Omega_{i-1} - 2\Omega_i}{\Delta\eta^2}\,\delta\right\}\left[1 + \beta_1\left(\frac{\Omega_{i+1} - \Omega_{i-1}}{2\Delta\eta}\right)^2\right] + f_i\frac{\Omega_{i+1} - \Omega_{i-1}}{2\Delta\eta} - M\sin^2\gamma\,\Omega_i$$

$$-K_p\Omega_i + (Fr+1)\Omega_i^2 + w(\theta_i - Nr\Omega_i - Rb\chi_i)\cos(\alpha) = 0, \tag{22}$$

$$\frac{\theta_{i+1}+\theta_{i-1}-2\theta_i}{Pr\Delta\eta^2}-\Omega_i\theta_i+f_i\frac{(\theta_{i+1}-\theta_{i-1})}{2\Delta\eta}+\frac{(\Phi_{i+1}-\Phi_{i-1})}{2\Delta\eta}Nb\,\theta_i$$

$$+Nt\left(\frac{\theta_{i+1}-\theta_{i-1}}{2\Delta\eta}\right)^2+M\,Ec\,\Omega_i^2=0, \tag{23}$$

$$\frac{\phi_{i+1}+\phi_{i-1}-2\phi_i}{\Delta\eta^2}-Sc\left(\Omega_i\phi_i+f_i\frac{(\Phi_{i+1}-\Phi_{i-1})}{2\Delta\eta}\right)+\frac{Nt}{Nb}\left(\frac{\theta_{i+1}+\theta_{i-1}-2\theta_i}{\Delta\eta^2}\right)=0, \tag{24}$$

$$\frac{\chi_{i+1}+\chi_{i-1}-2\,\chi_i}{\Delta\eta^2}-Lb\;\chi_i\Omega_i+Lb\left[\frac{(\chi_{i+1}-\chi_{i-1})}{2\Delta\eta}f_i\right]-Pe\left[\frac{(\chi_{i+1}-\chi_{i-1})}{2\Delta\eta}\frac{(\Phi_{i+1}-\Phi_{i-1})}{2\Delta\eta}\right]-Pe\,(\chi_i-$$

$$\Omega_i)\frac{\phi_{i+1}+\phi_{i-1}-2\phi_i}{\Delta\eta^2}=0. \tag{25}$$

In Eqs (22)–(25), all the terms can be treated as a current. Therefore, for the spatial discretized momentum Eq (22), the following currents are defined:

$$J_{i-1}=\left\{\frac{\Omega_{i-1}-\Omega_i}{\Delta\eta^2}\,\delta\right\}\left[1+\beta_1\left(\frac{\Omega_{i+1}-\Omega_{i-1}}{2\Delta}\right)^2\right], \tag{26}$$

$$J_{i+1}=\left\{\frac{\Omega_i-\Omega_{i-1}}{\Delta\eta^2}\,\delta\right\}\left[1+\beta_1\left(\frac{\Omega_{i+1}-\Omega_{i-1}}{2\Delta\eta}\right)^2\right], \tag{27}$$

$$J_{f,i}=f_i\frac{\Omega_{i+1}-\Omega_{i-1}}{2\Delta\eta}, \tag{28}$$

$$J_{M,i}=M\,sin^2\gamma\,\Omega_i+K_p\Omega_i, \tag{29}$$

$$J_{Fr,i}=(Fr+1)\Omega_i^2, \tag{30}$$

$$J_{Nr,i}=w(\theta_i-Nr\Omega_i-Rb\chi_i)c\,os(\alpha). \tag{31}$$

Then, by implementing Kirchhoff's law for electrical currents (J) from the circuit theory, the network model is obtained as follows:

$$J_{i-1}-J_{i+1}+J_{f,i}-J_{M,i}+J_{Fr,i}+J_{\alpha,i}=0. \tag{32}$$

Figure 2 shows the flow chart to obtain the numerical solution by means of the NSM for the momentum equation, which is similarly done for the other three equations. In the NSM technique, discretization of the differential equations is founded on the difference-finite formulation, where only a discretization of the spatial co-ordinates is necessary, with the time remaining as a real continuous variable.

A first-order central-difference approximation is used for the first derivate, and a *second-order* central difference approximation is used for the second derivate. The computational domain is divided into meshes, each of dimension $2\Delta\eta$ in η-space with an elemental cell thickness of 2Δη. This connecting requires equal potentials at the contact points of adjoining cells and equal outward-inward transference flows in adjoining elements. Recently, some meshless methods, such as the meshless local Petrov–Galerkin method [38], meshless Ritz method [39], meshless collocation method [40], meshless symplectic method [41], and element-free Galerking method [42], have been extended to solve similar problems.

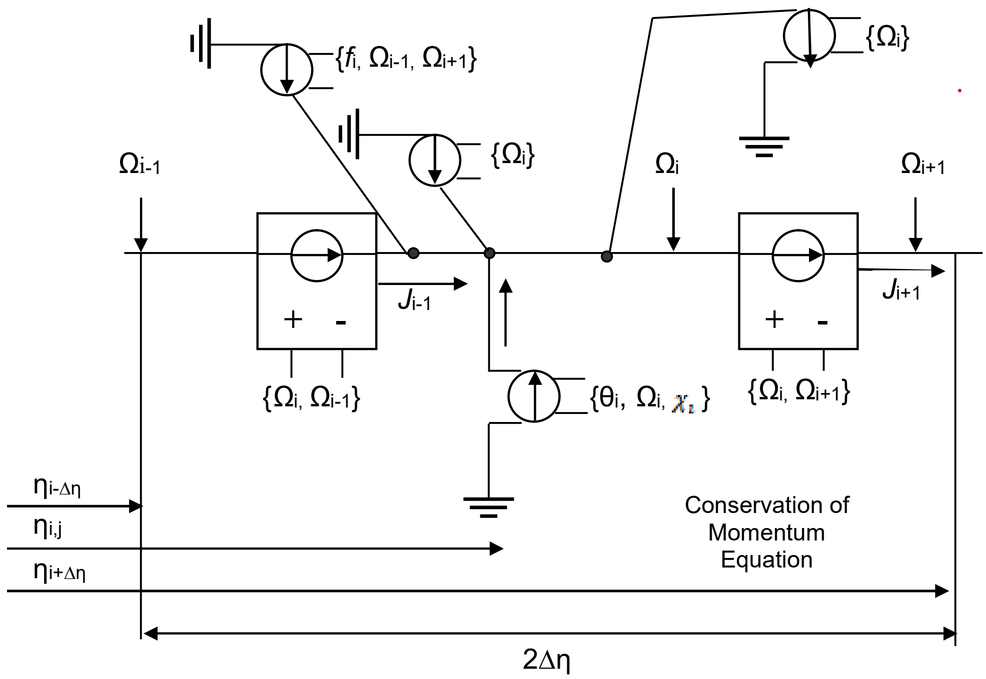

Figure 2. Network model of the elemental cell for the momentum Eq (21).

2.3. Matlab method of solution

A MATLAB finite difference solver called bvp4c is used to solve the Eqs (9)–(12) with the constraints (13). Equations (9)–(12) are converted into first order equations in order to apply this procedure. Setting $\Delta\eta = 0.0001$ is the size of the computing grid, and 10^{-6} is the relative tolerance. Equations (9)–(12) are reformulated into a system of first-order ODEs through the following variable substitutions:
Now, the transformed system of equations is expressed as follows:

$$y_3' = \left(\frac{1}{\delta(1+\beta y_3^2)}\right)\begin{pmatrix} -y_1y_3 + M\,sin^2(\gamma)\,y_2 + K_p y_2 - (Fr+1)y_2^2 \\ -w(y_4 - Nry_6 - Rby_8)\,cos(\alpha) \end{pmatrix}, \tag{34}$$

$$y_5' = Pr(y_4 - y_1y_5 - Nby_4y_7 - Nty_5^2) - MEcy_2^2, \tag{35}$$

$$y_7' = Sc(y_2y_6 + y_1y_7) - \frac{Nt}{Nb}Pr(y_4 - y_1y_5 - Nby_4y_7 - Nty_5^2), \tag{36}$$

$$y_9' = Lby_8y_2 - Lby_9y_1 + Pe\left(y_7y_9 + \begin{pmatrix} Sc(y_2y_6 + y_1y_7) \\ -\frac{Nt}{Nb}Pr\begin{pmatrix} y_4 - y_1y_5 - \\ Nby_4y_7 - Nty_5^2 \end{pmatrix} \end{pmatrix}(\chi + \Omega) \right). \tag{37}$$

The corresponding boundary conditions are given as follows:

$$\begin{cases} y_1(0) = S, y_2(0) = \in, y_4(0) = 1 - S_1, \\ y_6(0) = 1 - S_2, y_8(0) = 1 - S_3, \\ y_2(\infty) \to 0, y_4(\infty) \to 0, y_8(\infty) \to 0, \end{cases}. \tag{38}$$

2.4. Stability analysis and validation

The numerical reliability of the proposed formulation was assessed through grid-refinement consistency, cross-validation between two independent numerical procedures, and a comparison with previously published reference data. In particular, the computations were performed using two spatial step sizes, h = 0.001 and h = 0.0001, in order to examine the sensitivity of the solution to mesh refinement. Therefore, the comparison reported in Table 1 is interpreted as a practical grid-refinement convergence assessment of the finite-difference discretization adopted in the NSM formulation.

Table 1. Analysis of grid points.

$h = 0.0001$					$h = 0.001$				
η	$f'(\eta)$	$\theta(\eta)$	$\phi(\eta)$	$\chi(\eta)$	η	$f'(\eta)$	$\theta(\eta)$	$\phi(\eta)$	$\chi(\eta)$
0	0.2000	0.9000	0.9000	0.9000	**0**	0.2000	0.9000	0.9000	0.9000
0.4999	0.1050	0.8180	0.5096	−0.1647	**0.4990**	0.1051	0.8182	0.5102	−0.1638
0.8999	0.0695	0.6763	0.2905	−0.3891	**0.8990**	0.0696	0.6768	0.2909	−0.3889
1.9799	0.0010	0.0089	0.0030	−0.0130	**1.9790**	0.0010	0.0093	0.0031	−0.0136
1.9879	0.0006	0.0053	0.0018	−0.0079	**1.9870**	0.0006	0.0057	0.0019	−0.0084
1.9889	0.0005	0.0049	0.0016	−0.0072	**1.9880**	0.0006	0.0053	0.0018	−0.0078
2.0000	0.0000	0	0	0	**2.0000**	0.0000	0	0	0

Let Q_h denote a generic computed quantity obtained with a spatial step size of h, such as the wall gradients associated with momentum, heat transfer, nanoparticle concentration, or microorganism density. The relative grid-refinement variation may be expressed as follows:

$$\delta_Q = \frac{|\, Q_{h_1} - Q_{h_2} \,|}{\max\left(1, |\, Q_{h_2} \,|\right)}, h_1 = 0.001,\ h_2 = 0.0001.$$

A small variation between Q_{h1} and Q_{h2} indicates that further mesh refinement only produces minor changes in the computed engineering quantities. This supports grid-independent numerical behaviors within the tested discretization range.

In addition to the grid-refinement study, the NSM results were compared with those obtained using the collocation-based MATLAB solver bvp4c. This comparison provides an independent numerical cross-validation because both methods solve the same boundary-value problem using different computational frameworks. The agreement between the NSM and bvp4c solutions supports the numerical consistency of the present implementation.

Moreover, a benchmark validation was performed by comparing the present results with previously published data reported in Table 2. In this comparison, the additional physical parameters of the present model were set to the corresponding limiting values so that the formulation could be reduced to reference cases available in the literature. The agreement between the present MATLAB results, the NSM results, and the published data supports the reliability of the numerical procedure for the limiting configurations considered.

Table 2. Comparison of present and previous results on $f''(0)$ for $\delta = 1 Pr = 1, M = 2, \gamma = \frac{\pi}{2}, \epsilon = -1$ and the other parameters are taken zero.

S	Present study (Matlab)	Present study (NSM)	[15]	[14]
2	2.4142	2.4143	2.4143	2.4142
3	3.3028	3.3027	3.3027	3.3027
4	4.2361	4.2360	4.2360	4.2360

The truncation-error behavior of the NSM has also been examined by Solano et al. [43] for NSM-related integration schemes. Their analysis is used here as methodological support for the local behavior of the numerical integration procedure, not as a problem-specific global error estimate for the present boundary-value problem. In particular, Solano et al. [43] reported that the local truncation error of the trapezoidal rule scales as O(h^3), with $e_{n+1} = \frac{h^3}{6}\phi'''(t_n)$, whereas the second-order Gear/BDF scheme also exhibits an O(h^3) local contribution, with $e_{n+1} = \frac{h^3}{9}\phi'''(t_n)$.

Since no closed-form analytical solution is available for the coupled nonlinear bioconvective nanofluid problem considered here, no independent L_2- or L_∞-norm error bound is claimed. Therefore, the numerical support provided in the present work is based on the grid-refinement consistency, cross-validation between NSM and bvp4c, a benchmark comparison with previously published limiting cases, and the local truncation-error behavior reported for NSM-related integration schemes.

3. Discussion and results

The steady bioconvective flow of a Prandtl-type nanofluid over an inclined stretching sheet in a non-Darcy porous medium was analysed by varying key dimensionless parameters governing magnetic, porous, and biological transport effects. The coupled nonlinear system was solved using both the NSM and the bvp4c solver, ensuring numerical consistency prior to physical interpretation.

Figures 3–5 illustrate the influence of the magnetic parameter M on the velocity, temperature, and microorganism density profiles. An increase in M generates a stronger Lorentz force that opposes the fluid motion, thus leading to a significant reduction in the fluid velocity within the boundary layer region. This magnetic damping effect suppresses momentum transport and consequently increases the thickness of the hydrodynamic boundary layer. The retardation of the flow becomes more pronounced at higher values of M, thus indicating the dominant role of magnetic forces in controlling the fluid dynamics.

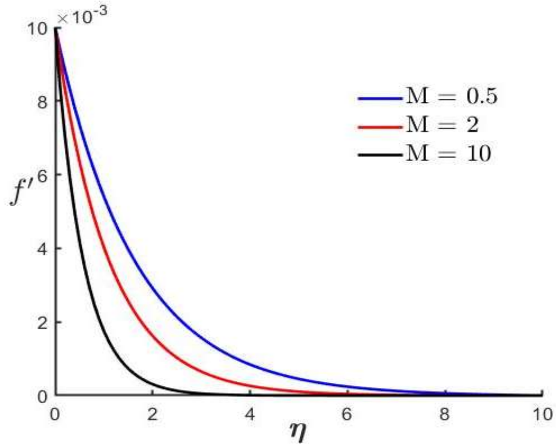

Figure 3. Impact of M on f'.

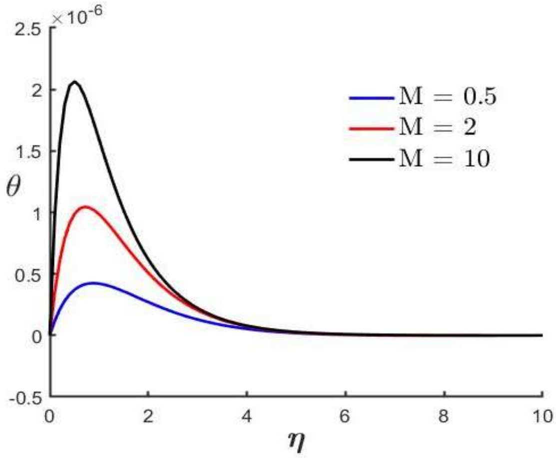

Figure 4. Variation of M on θ.

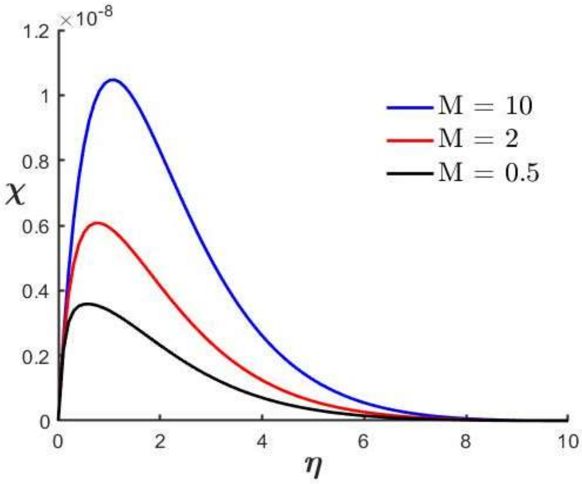

Figure 5. Impact of M on χ.

Furthermore, the enhanced magnetic resistance transforms part of the kinetic energy into thermal energy through Joule heating effects, which contributes to an increase in the temperature distribution throughout the flow field. As consequence, the thermal boundary layer thickness increases with increasing values of M. The elevated temperature field indicates a reduction in the rate of heat dissipation from the surface to the surrounding fluid.

In addition, the reduction in fluid velocity weakens the convective transport mechanism, thereby affecting the distribution of motile microorganisms within the fluid domain. Consequently, the microorganism density profile undergoes noticeable changes as the magnetic parameter increases. This behavior demonstrates the strong interaction between magnetic effects, momentum transport, thermal diffusion, and bioconvective processes. Overall, the magnetic parameter plays a crucial role in regulating the flow structure, heat transfer characteristics, and microorganism distribution in the system.

Figures 6–8 illustrate the influence of the bioconvection Lewis number L_b on the velocity gradient $f'(\eta)$, temperature, and microorganism density distributions. Since the surface shear stress is proportional to $f''(0)$, variations in L_b directly affect momentum transport within the boundary layer.

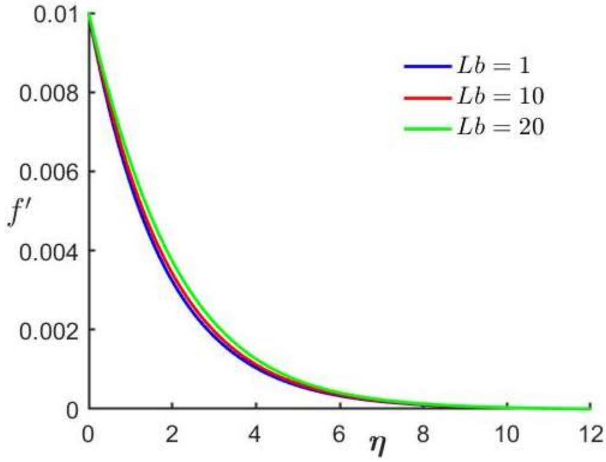

Figure 6. Impact of Lb on f'.

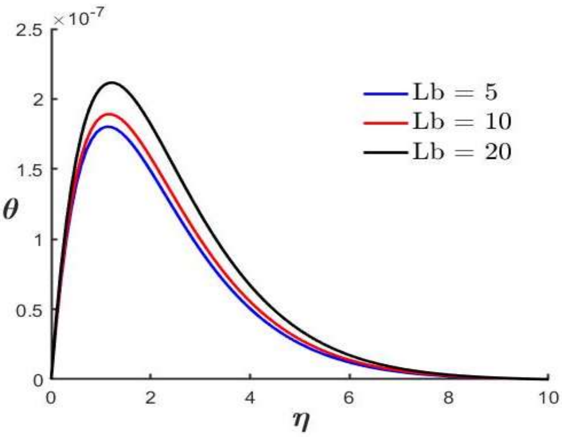

Figure 7. Impact of Lb on θ.

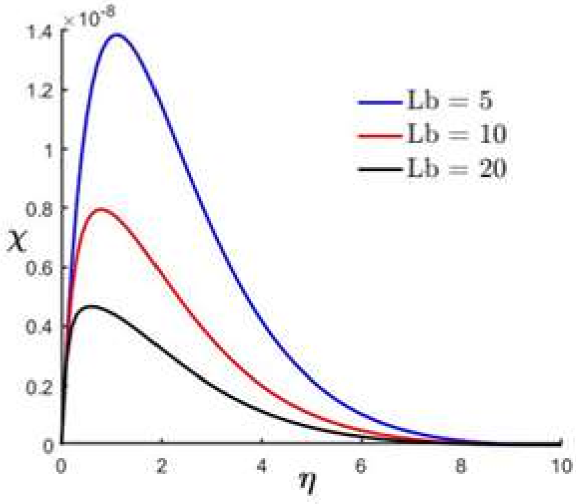

Figure 8. Impact of Lb on χ.

An increase in L_b, which represents enhanced microorganism diffusivity relative to momentum transport, weakens the intensity of bioconvective mixing within the fluid. As bioconvection becomes less dominant, the coupling between microorganism motion and fluid momentum is reduced, thus leading to a slight attenuation of the velocity profile throughout the boundary layer region. Consequently, the momentum boundary layer becomes thicker, and the fluid motion near the surface is significantly suppressed. Conversely, lower values of L_b strengthen microorganism-induced convection, thereby enhancing momentum transport and producing steeper velocity gradients near the surface. This intensified bioconvective activity promotes stronger fluid circulation and improves the interaction between the microorganisms and the surrounding flow field. Furthermore, variations in L_b significantly influence the overall stability and structure of the bioconvective flow, thus highlighting the important role of microorganism diffusivity in regulating the transport characteristics within the system.

The thermal field exhibits a complementary response. Higher values of L_b diminish microorganism-driven mixing, thereby reducing convective heat redistribution and allowing greater thermal accumulation near the wall. Consequently, the temperature profile increases in the near-surface region, and the thermal boundary layer becomes thicker. In contrast, stronger bioconvective mixing at lower values of L_b enhances heat transport away from the wall, thus resulting in lower temperature levels and a thinner thermal boundary layer. The stronger circulation generated by microorganism motion improves thermal diffusion and promotes a more uniform temperature distribution throughout the flow domain.

The microorganism density profile is particularly sensitive to L_b. Lower values of L_b intensify bioconvective accumulation mechanisms, thus leading to higher microorganism concentrations near the sheet. As L_b increases, enhanced diffusive effects dominate over advective accumulation, thus smoothing the density gradient and reducing peak microorganism concentration.

Overall, the bioconvection Lewis number plays a crucial role in regulating the balance between advective transport and microorganism diffusion, thereby modulating momentum, thermal, and biological boundary-layer structures in the nanofluid system. Furthermore, higher values of L_b suppress microorganism aggregation near the surface, thereby promoting a more uniform spatial distribution and enhancing the stability of the bioconvective flow regime.

Table 3 represents the behavior of $C_{fx}Re_x^{\frac{1}{2}}$, $Nu_xRe_x^{-\frac{1}{2}}$, and $Sh_xRe_x^{-\frac{1}{2}}$ for the variation of δ and β.

Table 3. Effect of δ and β on $Re_x^{\frac{1}{2}}C_{fx}$, $Re_x^{-\frac{1}{2}}Nu_x$, and $Re_x^{-\frac{1}{2}}Sh_x$.

$\boldsymbol{\delta}$	$\boldsymbol{\beta}$	$\boldsymbol{C_{fx}Re_x^{\frac{1}{2}}}$	$\boldsymbol{Nu_xRe_x^{-\frac{1}{2}}}$	$\boldsymbol{Sh_xRe_x^{-\frac{1}{2}}}$
0.5	1.0	0.2020	0.1532	1.6869
1.0	1.0	0.2878	0.1572	1.6681
1.5	1.0	0.3553	0.1585	1.6346
0.5	1.0	0.2020	0.1532	1.6363
0.5	1.5	0.2035	0.1534	1.6355
0.5	2.0	0.2044	0.1535	1.6346

This table summarizes the quantitative variation of the skin friction coefficient, Nusselt number, and Sherwood number with respect to changes in the inclination angle δ and the bioconvection parameter β; these quantities provide a direct measure of surface momentum transfer, thermal transport, and mass diffusion performance, respectively.

An increase in the inclination angle δ leads to a systematic rise in the skin friction coefficient. This behavior reflects the enhancement of the buoyancy component acting along the stretching surface, which intensifies the velocity gradients at the wall. The strengthened hydrodynamic shear directly increases the surface drag, thus confirming the strong sensitivity of wall shear stress to gravitational alignment.

The Nusselt number exhibits a similar increasing trend with the inclination angle, thus indicating enhanced heat transfer from the surface. The augmented buoyancy-driven flow intensifies convective transport within the thermal boundary layer, thereby increasing the temperature gradient at the wall. This demonstrates that geometric inclination plays a significant role in regulating the thermal performance in bioconvective porous systems.

In contrast, the Sherwood number shows a decreasing tendency as the inclination angle increases. Although buoyancy strengthens the overall convective motion, it simultaneously modifies the concentration boundary layer development in a manner that reduces the mass transfer rate at the surface. This inverse behavior highlights the nonlinear coupling between thermal and solutal transport mechanisms.

A comparable pattern is observed for variations in the bioconvection parameter. Increasing this parameter enhances the microorganism-induced convection, which strengthens the velocity gradients and consequently increases the skin friction coefficient. Additionally, the intensified mixing promotes heat transfer, thus leading to higher Nusselt numbers. These findings confirm that microorganism-driven bioconvection constitutes a non-negligible mechanism in the overall transport dynamics of the system and should therefore be carefully accounted for in the modeling of bioconvective porous flows.

However, the Sherwood number decreases with an increasing bioconvection parameter (β), indicating that stronger bioconvective mixing alters the concentration gradients near the wall and weakens the diffusive mass flux. This contrasting response between heat and mass transfer underscores the complex interplay between microorganism dynamics and solutal transport processes.

Overall, Table 3 quantitatively demonstrates that the inclination and bioconvection parameters exert a pronounced yet non-uniform influence on surface transport characteristics. The opposing behavior of thermal and mass transfer rates reflects the inherently coupled and nonlinear nature of MHD bioconvective nanofluid flow in non-Darcy porous media. These results reinforce the necessity of simultaneously considering both parameters when analyzing the surface transport phenomena, as their individual and combined effects give rise to competing mechanisms that cannot be adequately captured by simplified or decoupled modeling approaches.

Figures 9–11 present the variations of the Forchheimer parameter (Fr) on the velocity (f'), temperature (θ), and microorganism profile (χ). The Forchheimer parameter Fr represents nonlinear inertial resistance within the porous medium. An increase in Fr introduces additional drag forces that suppress fluid motion. As a consequence, the momentum transport decreases and the velocity boundary layer contracts. This leads to a noticeable falling in momentum, as shown in Figure 9. As Fr increases, the temperature (θ) slightly increases within the non-linear medium. Additionally, the peak temperature becomes higher. The thermal boundary layer becomes thicker. When the velocity decreases, heat stays longer in the fluid, so temperature rises, as presented in Figure 10.

In Figure 11, when Fr rises, the concentration of microorganisms (χ) decreases, the peak value becomes smaller, and the profile decays faster. Higher resistance reduces fluid motion, so microorganisms spread less. Increasing the Forchheimer number reduces the fluid velocity due to enhanced drag, which leads to a rise in temperature and a decline in microorganism distribution within the boundary layer. An increase in the Forchheimer number significantly suppresses the fluid motion (≈20% reduction), moderately enhances the thermal distribution (≈15% rise), and strongly diminishes the microorganism concentration (up to 70% reduction), thus highlighting its dominant control over the flow resistance and bio-convective transport.

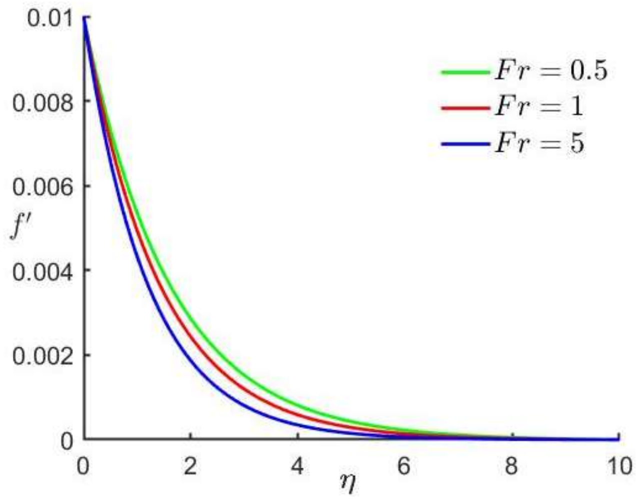

Figure 9. Impact of Fr on f'.

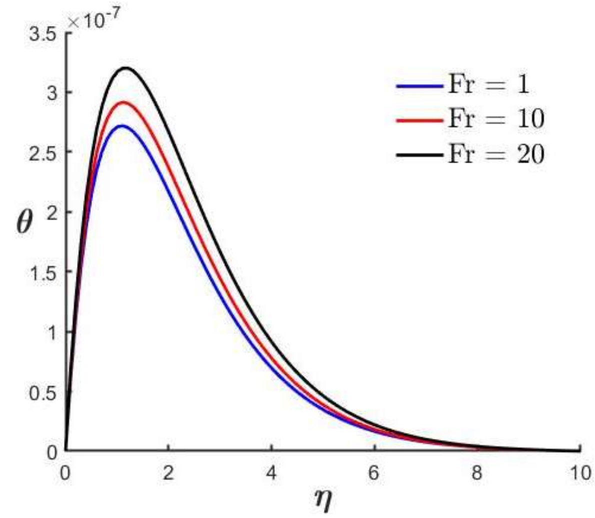

Figure 10. Impact of Fr on θ.

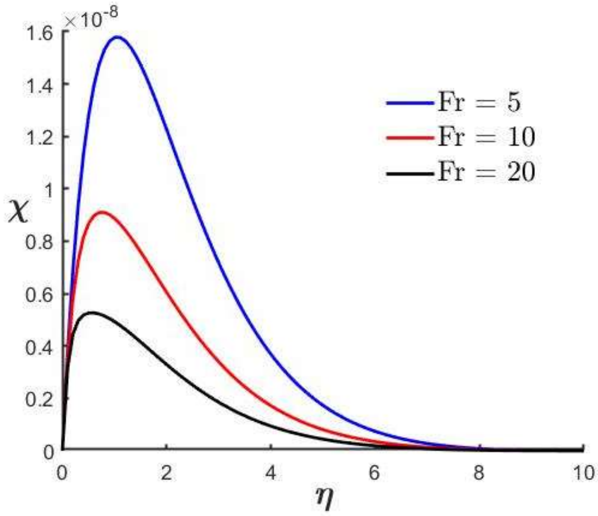

Figure 11. Impact of Fr on χ.

The reduction in convective intensity leads to an increased thermal retention within the fluid, thus slightly elevating the temperature profiles. Furthermore, the nonlinear drag alters the concentration gradients and reduces the Sherwood number, thus indicating a weakened mass transfer at the surface. These results demonstrate that inertial resistance in non-Darcy porous media plays a significant role in modulating both the hydrodynamic and bioconvective transport characteristics.

The small magnitudes observed in Figures 3–11 are a natural consequence of the boundary-layer behavior, in which all dependent variables $(f'(\eta), \theta(\eta), \phi(\eta), \chi(\eta))$ rapidly decay to zero as the similarity variable increases. This behavior is numerically confirmed by Table 1, where the computed values reduce to the order of 10^{-3} machine precision within a finite similarity domain $(\eta \approx 2)$. Consequently, the small values along the vertical axis reflect proper normalization combined with strong damping effects arising from magnetic and porous resistance, and are fully consistent with both the physical assumptions and the mathematical formulation of the problem.

The numerical solutions obtained via the NSM were found to be in excellent agreement with those computed using the collocation-based bvp4c solver. Grid refinement tests confirmed that the computed profiles remain invariant within the prescribed tolerance limits. This agreement validates the electrical analogy formulation and confirms the robustness of the NSM implementation for strongly nonlinear, coupled boundary-layer systems.

4. Conclusions

The principal findings of the present investigation on MHD bioconvective flow of a Prandtl-type nanofluid in a non-Darcy porous medium may be summarized as follows:

1. The magnetic parameter significantly suppresses the velocity profile due to the Lorentz force effects, while simultaneously increasing the thermal boundary layer thickness and enhancing microorganism accumulation in the near-wall region.
2. The Forchheimer parameter intensifies the inertial resistance within the porous medium, thus leading to a reduced momentum transport and noticeable modifications in both the temperature and concentration distributions.
3. Variations in the bioconvection Lewis number alter the microorganism density profiles and influence coupled heat and mass transfer mechanisms, thus reflecting the strong nonlinear interaction between biological and hydrodynamic transport processes.
4. The inclination angle and bioconvection parameter increase the surface shear stress and heat transfer rates, whereas increasing the porous resistance reduces the Sherwood number, thus indicating weakened mass diffusion near the wall.
5. Cross-validation between the collocation-based bvp4c solver and the NSM confirms numerical consistency, thereby demonstrating that the NSM formulation provides a stable and robust computational framework for strongly nonlinear multiphysics boundary-layer systems.
6. Therefore, $\boldsymbol{Fr}$ acts as an adaptable parameter that decelerates fluid motion while endorsing heat growth and restricting microorganism dispersion, which is highly important in applications that involve porous media flows, bio-convection, and thermal management systems.
7. The electrical network representation inherent to the NSM naturally enforces conservation principles through Kirchhoff's current law and accommodates nonlinear source terms without prior linearization, thereby supporting its applicability to complex bioconvective nanofluid configurations.

The present framework may be extended to unsteady flows, non-similar boundary conditions, and alternative non-Newtonian rheological models, thus offering a versatile computational approach for advanced coupled transport phenomena in porous media. Therefore, future work should include extended benchmark validation against experimental data and established CFD and heat transfer numerical methods in order to further evaluate the robustness, stability, and general applicability of the proposed approach. Besides, other extensions of this work may consider unsteady or time-dependent flow behaviors, which are important in pulsatile biological processes and transient thermal systems. Additional investigations could incorporate alternative non-Newtonian rheological models, such as Casson, Carreau, Williamson, or viscoelastic fluids, to better capture the behavior of complex biological and polymeric suspensions under varying flow conditions.

Author contributions

S. Ahmed has contributed to draw the flow diagram and all the figures, also verify the manuscript; N. J. Hazarika has explored the result and discussion section and other mathematical part; J. Zueco has checked the numerical results and provided comments in the discussion section; J. Solano has developed the network models and obtained the numerical solutions with NSM. All the authors have discussed the results, reviewed and approved the final version of the manuscript.

Use of Generative-AI tools declaration

The authors declare they have not used Artificial Intelligence (AI) tools in the creation of this article.

Conflict of interest

The authors declare no conflict of interest.

References

1. S. Biswas, S. Mahato, J. Dhar, A review on microbial bioconvection in porous media: Mechanisms, bloom formation, and technological Frontiers, *Int. Comm. Heat Mass Trans.*, **167** (2025), 109394. https://doi.org/10.1016/j.icheatmasstransfer.2025.109394
2. O. A. Bég, V. R. Prasad, B. Vasu, Numerical study of mixed bioconvection in porous media saturated with nanofluid containing oxytactic microorganisms, *J. Mech. Med. Biol.*, **13** (2013). https://doi.org/10.1142/S021951941350067X
3. M. Priyadharsini, D. M. Gururaj, Bioconvection effects on the heat and mass transfer of unsteady MHD blood flow over a permeable artery, *Numer. Heat Tr. B-Fund.,* **86** (2025), 326–352. https://doi.org/10.1080/10407790.2023.2282168
4. H. Waqas, M. Imran, T. Muhammad, On bio-convection thermal radiation in Darcy–Forchheimer flow of nanofluid with gyrotactic motile microorganism under Wu's slip over stretching cylinder/plate, *Int. J. Numer. Meth. Fl.*, **31** (2021), 1520–1546. https://doi.org/10.1108/HFF-05-2020-0313
5. A. Ahmad, M. Ashraf, K. Ali, Bioconvection due to gyrotactic microbes in a nanofluid flow through a porous medium, *Heliyon*, **6** (2020), e05832, https://doi.org/10.1016/j.heliyon.2020.e05832
6. J. Wang, Z. Mustafa, I. Siddique, Computational analysis for bioconvection of microorganisms in PPrandtl nanofluid Darcy–Forchheimer flow across an inclined sheet, *Nanomaterials*, **12** (2022), 1–16. https://doi.org/10.3390/nano12111791
7. M. Yaseen, S. K. Rawat, M. Kumar, Cattaneo–Christov heat flux model in Darcy–Forchheimer radiative flow of MoS_2–SiO_2/kerosene oil between two parallel rotating disks, *J. Therm. Anal. Calorim.*, **147** (2022), 10865–10887. https://doi.org/10.1007/s10973-022-11248-0
8. W. A. Khan, O. D. Makinde, Z. H. Khan, MHD boundary layer flow of a nano fluid containing gyrotactic microorganisms past a vertical plate with Navier slip, *Int. J. Heat Mass Transf.,* **74** (2014), 285–291. https://doi.org/10.1016/j.ijheatmasstransfer.2014.03.026

9. I. Khan, A. Hussain, M. Y. Malik, S. Mukhtar, On magnetohydrodynamics Prandtl fluid flow in the presence of stratification and heat generation, *Physica A*, **540** (2020), 123008. https://doi.org/10.1016/j.physa.2019.123008
10. B. Das, S. Ahmed, Numerical modeling of bioconvection and heat transfer analysis of Prandtl nanofluid in an inclined stretching sheet: A finite difference scheme, *Numer. Heat Tr. A- Appl.*, **85** (2024), 3431–3451. https://doi.org/10.1080/10407782.2023.2237184
11. S. Hazarika, S. Ahmed, Physical Insights on bio-convection in Prandtl nanofluid over an inclined stretching sheet in non-Darcy medium: Numerical simulation, *Sci. Iran.,* **32** (2023), 8125. https://doi.org/10.24200/sci.2023.62949.8125
12. H. U. Rasheed, S. Islam, J. Khan, T. Abbas, M. I. Mohmand, Numerical solution of chemically reactive and thermally radiative MHD Prandtl nanofluid over a curved surface with convective boundary conditions, *ZAMM-J. Appl. Math. Mech.*, **106** (2021). https://doi.org/10.1002/zamm.202100125
13. A. Abbas, R. Shafqat, M. B. Jeelani, N. H. Alharthi, Convective heat and mass transfer in third-grade fluid with Darcy–Forchheimer relation in the presence of thermal-diffusion and diffusion-thermo effects over an exponentially inclined stretching sheet surrounded by a porous medium: A CFD study, *Processes*, **10** (2022), 776. https://doi.org/10.3390/pr10040776
14. M. Bilal, M. Nazeer, Numerical analysis for the non-Newtonian flow over stratified stretching/shrinking inclined sheet with the aligned magnetic field and nonlinear convection, *Arch. Appl. Mech.*, **91** (2021), 949–964. https://doi.org/10.1007/s00419-020-01798-w
15. K. Bhattacharyya, Effects of heat source/sink on MHD flow and heat transfer over a shrinking sheet with mass suction, *Chem. Eng. Res. Bull.*, **15** (2011), 12–17. https://doi.org/10.3329/cerb.v15i1.6524
16. R. Ghosh, T. M. Agbaje, S. Mondal, S. Shaw, Bio-convective viscoelastic Casson nanofluid flow over a stretching sheet in the presence of induced magnetic field with Cattaneo-Christov double diffusion, *Int. J. Biomath.,* **15** (2022), 2150099. https://doi.org/10.1142/S1793524521500996
17. M. Jawad, A. Saeed, A. Khan, S. Islam, MHD bioconvection Darcy–Forchheimer flow of Casson nanofluid over a rotating disk with entropy optimization, *Heat Transf.*, **50** (2021), 2168–2196. https://doi.org/10.1002/htj.21973
18. B. K. Siddiqui, S. Batool, M. Y. Malik, Q. M. Ul Hassan, A. S. Alqahtani, Darcy Forchheimer bioconvection flow of Casson nanofluid due to a rotating and stretching disk together with thermal radiation and entropy generation, *Case Study Therm. Eng.*, **27** (2021), 101201, 1–12. https://doi.org/10.1016/j.csite.2021.101201
19. U. Habib, S. Abdal, I. Siddique, R. Ali, A comparative study on micropolar, Williamson, Maxwell nanofluids flow due to a stretching surface in the presence of bioconvection, double diffusion and activation energy, *Int. Comm. Heat Mass Transf.*, **127** (2021), 105551. https://doi.org/10.1016/j.ijft.2026.101592
20. M. Batool, S. Akhter, S. Ahmad, M. Ashraf, K. Ali, Impact of viscous dissipation on MHD Darcy-Forchheimer nano liquid flow comprising gyrotactic microorganisms past a nonlinear extending surface, *Sci. Iran.*, **30** (2022), 2235–2244. https://doi.org/10.24200/sci.2022.59018.6018
21. U. Farooq, T. Liu, U. Farooq, S. Majeed, Non-similar analysis of bioconvection MHD micropolar nanofluid on a stretching sheet with the influences of Soret and Dufour effects, *Appl. Water Sci.*, **4** (2024), 1–14. https://doi.org/10.1007/s13201-024-02143-0

22. U. Farooq, M. Hussain, U. Farooq, Non-similar analysis of chemically reactive bioconvective Casson nanofuidfow over an inclined stretching surface, *ZAMM J. Appl. Math. Mech.,* **104** (2023), e202300128. https://doi.org/10.1002/zamm.202300128
23. U. Farooq, L. Tao, Non-similar analysis of MHD bioconvective nanofluid flow on a stretching surface with temperature-dependent viscosity, *Num Heat Tr. A-Appl.*, **83** (2023), 1353–1369. https://doi.org/10.1080/10407782.2023.2279249
24. M. A. Mansour, A. M. Rashad, B. Mallikarjuna, A. K. Hussein, M. Aichouni, L. Kolsi, MHD mixed bioconvection in a square porous cavity filled by gyrotactic microorganisms, *Int. J. Heat Technol.*, **37** (2019), 433–445. https://doi.org/10.18280/ijht.370209
25. K. Naganthran, M. F. Basir, T. Thumma, E. O. Ige, R. Nazar, I. Tlili, Scaling group analysis of bioconvective micropolar fluid flow and heat transfer in a porous medium, *J. Therm. Anal. Calorim.*, **143** (2021), 1943–1955. https://doi.org/10.1007/S10973-020-09733-5
26. B. Das, S. Ahmed, Numerical modeling of bioconvection and heat transfer analysis of Prandtl nanofluid in an inclined stretching sheet: A finite difference scheme, *Num. Heat Tr. A-Appl*., 2023. https://doi.org/10.1080/10407782.2023.2237184
27. M. M. Khader, M. Adel, Investigation of Reiner–Philippoff nanofluid flow over a stretching sheet considering diffusion and first order velocity slip: Numerical and theoretical analysis*, ZAMM-J. Appl. Math. Mech.,* **15** (2025). https://doi.org/10.1002/zamm.70245
28. N. I. Nima, M. A. Hannan, Mixed bioconvection flow around a vertical thin needle with variable surface fluxes, *Dynamics*, **5** (2025), 1–21. https://doi.org/10.3390 /dynamics5010002
29. M. Jawad, A. Majeed, W. Abdelfattah, G. Bognár, S. Kamangar, A. S. Hendy, Dynamics of activation energy and gyrotactic microorganisms on radiative Williamson nanofluid with Soret and Dufour bounded by porous nonlinearly stretching surface, *J. Radiation Res. Appl. Sci.,* **18** (2025), 101525. https://doi.org/10.1016/j.jrras.2025.101595
30. S. Sankari, M. E. Rao, A. M. A. Elsiddieg, W. Khan, O. D. Makinde, T. Saidani, et al., Analytical solution of MHD bioconvection Williamson nanofluid flow over an exponentially stretching sheet with the impact of viscous dissipation and gyrotactic microorganism, *Plos One*, **20** (2025), https://doi.org/10.1371 /journal.pone. 0306358
31. M. M. Khader, M. Adel, M. M. Babatin, A. Alaidrous, Williamson nanofluid flow and thermal transfer generated by a convectively heated stretched sheet via Fibonacci-Lucas polynomials, *AIMS Math.*, **10** (2025), 29012–29036. https://doi.org/10.3934/math.20251276
32. L. W. Nagel, *SPICE2: A computer program to simulate semiconductor circuits*, Ph.D. Thesis, University of California, Berkeley, CA, USA, 1975.
33. L. Nagel, D. Pederson, *Simulation program with integrated circuit emphasis*, In Proceedings of the Midwest Symposium on Circuit Theory, Waterloo, ON, Canada, 1973.
34. S. Ahmed, K. Karabi, J. Zueco, Nonlinear magnetohydrodynamic radiating flow over an infinite vertical plate in a saturated porous medium Laplace and numerical approaches, *J. Eng. Phys. Therm.*, **87** (2014), 1169–1182. https://doi.org/10.1007/s10891-014-1124-z
35. J. Zueco, L. M. López-González, Network model to study physiological processes of hypobaric decompression sickness: New numerical results, *Acta Astronaut.*, **121** (2016), 256–270. https://doi.org/10.1016/j.actaastro.2015.12.051

36. S. Ahmed, J. Zueco, L. M. López-González, Effects of chemical reaction, heat and mass transfer and viscous dissipation over a MHD flow in a vertical porous wall using Perturbation method, *Int. J. Heat Mass Transf.,* **104** (2017), 409–418. http://dx.doi.org/10.1016/j.ijheatmasstransfer.2016.07.076
37. B. Das, S. Ahmed, J. Zueco, Bioconvective flow characteristics of NEPCM–water nanofluid over an inclined cylinder in porous medium: An extended Darcy model approach, *Mathematics*, **12** (2024), 1–18. https://doi.org/10.3390/math12244012
38. M. Dehghan, D. Mirzaei, The meshless local Petrov–Galerkin (MLPG) method for the generalized two-dimensional non-linear Schrödinger equation, *Eng. Anal. Bound. Elem.,* **32** (2008), 747–756. https://doi.org/10.1016/j.enganabound.2007.11.005
39. L. W. Zhang, K. M. Liew, An element-free based solution for nonlinear Schrödinger equations using the ICVMLS-Ritz method, *Appl. Math. Comp.,* **249** (2014), 333–345. https://doi.org/10.1016/j.amc.2014.10.033
40. R. Jiwari, S. Kumar, R. C. Mittal, J. Awrejcewicz, A meshfree approach for analysis and computational modeling of non-linear Schrödinger equation, *Comp. Appl. Math.,* **39** (2020). https://doi.org/10.1007/s40314-020-1113-0
41. S. L. Zhang, Meshless symplectic and multi-symplectic local RBF collocation methods for nonlinear Schrödinger equation, *J. Comput. Phys.,* **450** (2022). https://dl.acm.org/doi/10.1007/s00366-024-02071-2
42. X. Li, H. Dong, Unconditional error analysis of an element-free Galerkin method for the nonlinear Schrödinger equation, *Comm. Nonlin. Sci. Num. Simul.,* **151** (2025) 109103. https://doi.org/10.1016/j.cnsns.2025.109103
43. J. Solano, J. Mulas-Pérez, F. Balibrea, J. A. Moreno-Nicolás, Truncation error of the network simulation method: Chaotic dynamical systems in mechanical engineering, *Mathematics*, **12** (2024), 1–19. https://doi.org/10.3390/math12213441

AIMS Press